Applied Physics Letters ARTICLE scitation.org/journal/apl

Topological valley states in sonic crystals with Willis coupling

Cite as: Appl. Phys. Lett. **119**, 051903 (2021); doi: 10.1063/5.0055789
Submitted: 3 May 2021 · Accepted: 29 July 2021 ·
Published Online: 5 August 2021

View Online Export Citation CrossMark

Hongfei Qu, Xiaoning Liu,[a] and Gengkai Hu

AFFILIATIONS

Key Laboratory of Dynamics and Control of Flight Vehicle, Ministry of Education, School of Aerospace Engineering, Beijing Institute of Technology, Beijing 100081, China

[a]Author to whom correspondence should be addressed: liuxn@bit.edu.cn

ABSTRACT

Acoustic media with Willis coupling possess intrinsic directionality owing to the vector nature of coupling coefficients in constitutive relations. Here, we report a type of sonic topological insulator that exhibits the valley Hall effect by using an acoustic fluid of the Willis type. We find that the valley Hall phase transition can be triggered by tuning the coupling vector. In addition, the Dirac cones or valley position are displaced away from high symmetry points in the Brillouin zone. The tunability of the valley offset offered by Willis coupling helps to realize equally robust one-way transport for both zigzag and armchair domain walls and for more tortuous wave channels.

Published under an exclusive license by AIP Publishing. https://doi.org/10.1063/5.0055789

Topological phases (TPs) and topologically protected transport phenomena have in recent decades been a vibrant area of research in various branches of science. One of the most impressive features of such phenomena is the existence of edge states, which are immune to defects and sharp corners, between domains characterized by distinct topological invariants.[1] Since its advent in condensed matter physics,[2–4] this paradigm has been extended to classical wave systems, such as electromagnetic,[5–8] acoustic,[9–15] and mechanical waves.[16–22] A number of topological wave transport and other applications, such as low-loss devices, waveguides, and information carriers, have been theoretically explored and experimentally demonstrated.[9,10,15,16]

For acoustic waves, TPs can be generated via either active or passive processes that produce the acoustic versions of the Floquet/Chern insulator or the quantum spin Hall effect, respectively, for which the energy band topology is defined for an entire band. In addition, another type of TP, namely, the valley Hall effect (VHE),[23,24] can be formed via the locally nontrivial topology of the band structure. The VHE is created based on single Dirac cones, which are usually located at high-symmetry points in the first Brillouin zone (BZ), e.g., the BZ corners at which the point group of wave vectors possesses C_{3v} symmetry. When the symmetry is perturbed to a lower state, the twofold degeneracy may be lifted and split into valley states carrying opposite pseudospins. A number of methods, such as scatterer rotation or acoustic resonators, can be used to engineer acoustic Dirac cones and the VHE. Recent studies show that the VHE also encompasses Dirac cones away from high-symmetry points,[25–27] revealing the possibility of structural design with lower symmetry.

Existing methods for acoustic VHEs mostly concentrated on the geometry or the lattice arrangement of scatterers.[10,14–16] However, acoustic TPs have not been reported to be related to the constitutive behaviors of either host media or scatterers in sonic crystals (SCs). In this Letter, we report the VHE in an acoustic medium with Willis coupling,[28–30] which is also known as bi-anisotropy since it introduces a relationship between pressure (momentum) and particle velocity (strain), in direct analogy to magneto-electric coupling.[31] Willis coupling was explored in the 1980s for elastodynamics and revisited in recent years in context of metamaterials, since it not only provides a physically meaningful description for various metamaterials[32,33] but also offers extra dimensions in designing exotic wave functionalities, e.g., full control of acoustic meta-surfaces[34] and asymmetric transport,[35,36] among others. It should be emphasized here that the acoustic Willis coupling has only been observed in discrete meta-atoms, such as the membrane unit,[33,37] folded channel,[38] or C-ring resonator,[39] but not in continuous media. Realization of the theoretical results of this work will be considered in the future work.

As depicted in Fig. 1(a), we consider a two-dimensional SC consisting of a triangular lattice of hard sound scatterers of circular shape with radius r immersed in an air matrix, where a hexagonal unit cell and lattice vectors ($\mathbf{a}_1$, $\mathbf{a}_2$) are marked. In Fig. 1(b), the black line shows the band structure of this simple SC. In the calculation, $a = |\mathbf{a}_1| = 4.3$ cm, $r = 1.25$ cm, air density $\rho = 1.29$ kg/m^3, and the speed of

Published under an exclusive license by AIP Publishing

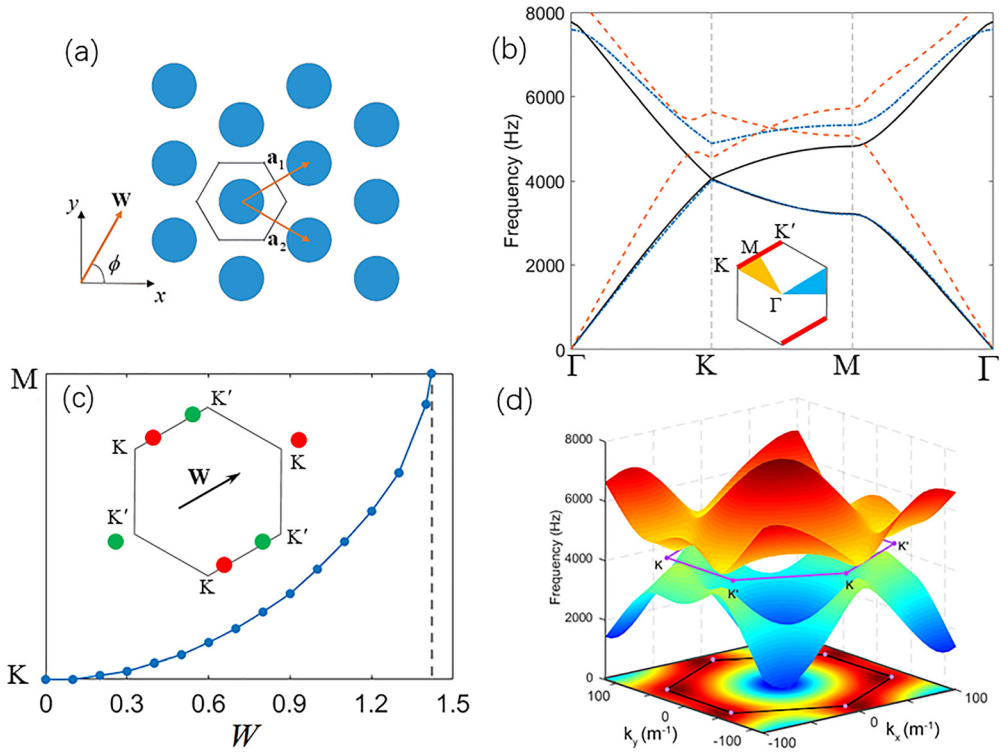

FIG. 1. (a) Triangular array of circular scatterers immersed in a Willis fluid featuring a coupling vector **W**. (b) Band diagram of the SC without Willis coupling (black), and with $W = 1$ and $\phi = \pi/6$ (the blue and orange lines trace different paths in BZ as depicted in the inset using the same colors). (c) Movement of the Dirac degeneracies along the high symmetry edge of BZ, from the corner to the middle, as a function of the coupling magnitude W. The inset exemplifies the moving pattern for $\phi = \pi/6$. (d) 3D band structure of a SC with Willis coupling $W = 1$ and $\phi = \pi/3$, showing an omnidirectional bandgap, and the offset of the valley can be seen by the projection plot of the first band.

sound $c = 343$ m/s. As expected, due to the $C_{6v}(C_{3v})$ symmetry of the direct (reciprocal) space, deterministic single Dirac cones are found for the first two bands at the K and K′ points of BZ at 4550 Hz. To lift the cone and create valleys carrying distinct topological charges, it is common to use scatterers with lower (e.g., triangular[10]) symmetry and rotate them to break the C_{3v} symmetry of K(K′) to C_3. However, for the circular scatterers as we consider here, rotation would not break the degeneracy. Here, we propose another route: an investigation of the effect of the Willis polarization in the background medium containing scatterers with C_{6v} symmetry.

This is achieved by replacing the matrix fluid with a Willis medium, which is characterized by the following constitutive relation:

$$\begin{cases} -p = \kappa\varepsilon + \mathbf{S}\cdot\mathbf{v}, \\ \boldsymbol{\mu} = \rho\mathbf{v} + \mathbf{S}\varepsilon, \end{cases} \tag{1}$$

where p is the acoustic pressure, ε is the volumetric strain, $\mathbf{v}$ is the particle velocity, $\boldsymbol{\mu}$ is the momentum density, and κ is the bulk modulus. $\mathbf{S}$ represents the Willis coupling term, which is a vector for acoustic fluids. The vector feature of $\mathbf{S}$ renders the SC matrix naturally directional and, thus, provides another way to reduce the symmetry of system. For convenience, we define a non-dimensional quantity $\mathbf{W} = i\mathbf{S}/\sqrt{\kappa\rho}$ that is purely real for a lossless Willis medium in the absence of non-local effects.[32] The directionality of the matrix medium is characterized by $W = |\mathbf{W}|$ and the azimuthal angle ϕ [Fig. 1(a)]. The system with Willis coupling was numerically analyzed using COMSOL Multiphysics.[40]

In Fig. 1(b), the first two bands of the SC with coupling parameters $W = 1$ and $\phi = \pi/6$ are shown in blue along the Γ-K-M-Γ path. Compared to the case without Willis coupling, it seems that the degeneracy at the BZ corners has been lifted and a gap has emerged. However, the bandgap is not omnidirectional. Since the C_3 symmetry is not preserved, when we follow the inequivalent path Γ-K-M-Γ as shown in Fig. 1(b) by the orange lines, it is seen that a Dirac cone still exists but is offset to the BZ edge. The existence of shifted Dirac cones in the presence of a Willis coupling vector of a particular direction can be explained by the **k**·**p** effective Hamiltonian and the group theory.[41] The coupling vectors along $\phi = n\pi/6$, with n being an integer reduce the SC symmetry in direct space from C_{3v} to C_s with the mirror plane collinear with **W**. However, only those along $\phi = (2n+1)\pi/6$ support **k**-points on a pair of BZ edges [highlighted as red in the inset of Fig. 1(b)] with C_s symmetry, i.e., they map **k** to equivalent $\mathbf{k}+\mathbf{b}$ points upon a reflection, with **b** being a reciprocal lattice vector.[42] Actually, the original cones move from the corner toward M points of those edges, and considering translational symmetry of the BZ, the pattern of cone locations is sketched by the inset to Fig. 1(c) for $\phi = \pi/6$, which shows the calculated movement of cones along the BZ edge as a function of W. The degenerate points move from K(K′) toward M as W increases. When W is larger than a critical value (1.42 for the case shown), the cones from the K and K′ corners meet and disappear, and

Published under an exclusive license by AIP Publishing

thus, a bandgap is opened up. It is interesting that reversing the coupling vector $\mathbf{W}$ to $-\mathbf{W}$ does not change the cone pattern or the band structure of the SC. This feature holds even for a general ϕ that lifts degeneracy. For $\phi \neq (2n+1)\pi/6$, depending on the magnitude and direction of $\mathbf{W}$, the Dirac cones will be lifted to create extrema whose projection onto the BZ deviate around corresponding K (K′) points. Figure 1(d) shows the 3D band surfaces with $W=1$ and $\phi = \pi/3$. Here, we refer to the extrema as K(K′) valleys, where their shifted locations can be recognized by the density plot of the first band shown in the figure.

We further investigated the vortex chirality of the valley state. Figure 2 presents the variation of frequency extrema for the first two bands near the K′-valley vs the angle ϕ. It is obvious that the two bands are locked with opposite vortex pseudospins, and band inversion occurs every time the gap closes and reopens at $\phi = (2n+1)\pi/6$, signaling a TP transition in a VHE insulator. The eigenstates selectively shown for $\phi = \pi/3$ and $4\pi/3$ are the pressure amplitude, and the arrows indicate the spatial distribution of the time-averaged Poynting vectors $\mathbf{I} = \mathrm{Re}(p\mathbf{v}^*)/2$. The vortex profiles are clearly visible, yet the vortex cores also deviate from the corners of a standard unit cell. The two valley states are labeled by p^+ and q^-, corresponding to the two inequivalent lattice sites, which are adjacent to energy flow in the direction indicated by the sign. In Fig. 2, we focus on the physics at the K′-valley, while the counterparts at the K-valley possess invariant vortex core locations but opposite chirality as required by the time-reversal symmetry.

The bulk band topology of a VHE insulator is characterized by the valley Chern number, which is the local integral of the Berry curvature around a valley. The Berry curvature, endowing a bulk band with geometric structure, is defined via $\Omega(\mathbf{k}) = i\nabla_{\mathbf{k}} \times \langle\psi(\mathbf{k})|\ \nabla_{\mathbf{k}}|\psi(\mathbf{k})\rangle$, where ψ is the eigenstate on the band and $\nabla_{\mathbf{k}}$ is the $\mathbf{k}$-space gradient.[1]

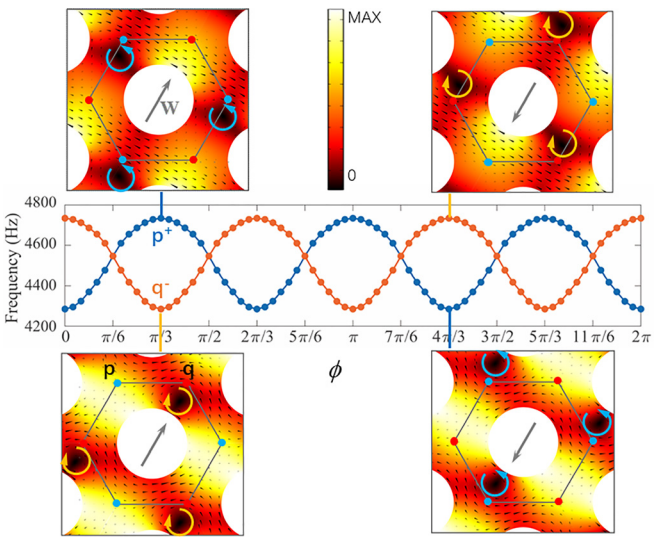

FIG. 2. TP transition and band inversion at the K′-valley as a function of ϕ. Valley states with pseudospin "+" and "−" (indicated in the inset with energy vortices and field intensity) lock with specific bands and exchange their position when the bands across the degenerate point at $\phi = (2n+1)\pi/6$. Energy vortex cores are displaced around the lattice site according to the direction of $\mathbf{W}$.

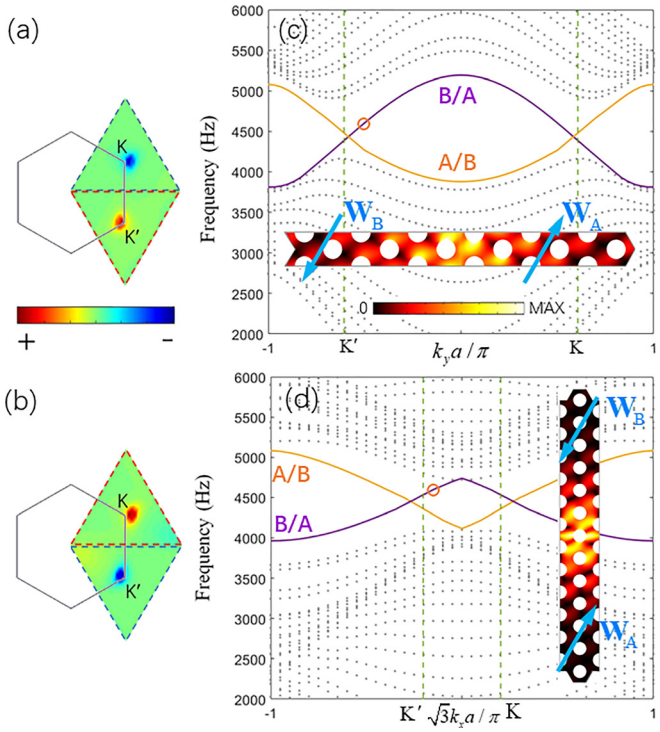

FIG. 3. Density plots of Berry curvature for (a) the 1st (2nd) band and (b) the 2nd (1st) band of phase A(B); the dashed boundary indicates the integration area for evaluation of the valley Chern number. Projected band structures for a zigzag domain wall along the *y*-direction (c) and armchair domain wall along the *x*-direction (d). The insets demonstrate the eigenstates corresponding to the circles on the band, and the vertical dashed green lines mark the projected valley positions.

Figures 3(a) and 3(b) present the numerically evaluated Berry curvature for the 1st and 2nd bands for $\phi = \pi/3$, respectively. We observe that the nonzero Berry curvature still concentrates to the valleys and decays quickly away from them, as is typical of VHE insulators. The upper and lower bands of distinct valleys carry opposite Berry curvatures, implying that a pair of non-trivial valley Chern numbers $C_v = \mp(\pm)1/2$, evaluated by integrating the Berry curvature over half of the BZ, can be assigned to index the K (K′) valley. It is also observed that the valley position displaces from the K (K′) point as ϕ varies. This feature of a displaced valley will subtly play a role on the interface mode along different types of domain walls, as shown later. For the same SC array with $\mathbf{W}$ reversed ($\phi = 4\pi/3$), the valley position remains the same as in Figs. 3(a) and 3(b); however, the valley Chern numbers at each valley will reverse their signs.

We next examine the existence of interface modes required by the bulk-edge correspondence at a domain wall between VHE phases with distinct topological indices, taking phase A ($\phi = \pi/3$) and phase B ($\phi = 4\pi/3$) as an example. Figures 3(c) show the projected band structure of a strip supercell composed of the two phases divided by a *zigzag* domain wall along the *y*-direction in which dotted and solid lines represent bulk and interface modes, respectively. An interface band with configuration A/B (phase A on the left and B on the right) is shown in orange and that with reversed configuration B/A is shown in purple. The inset illustrates the field intensity of an interface state

Published under an exclusive license by AIP Publishing

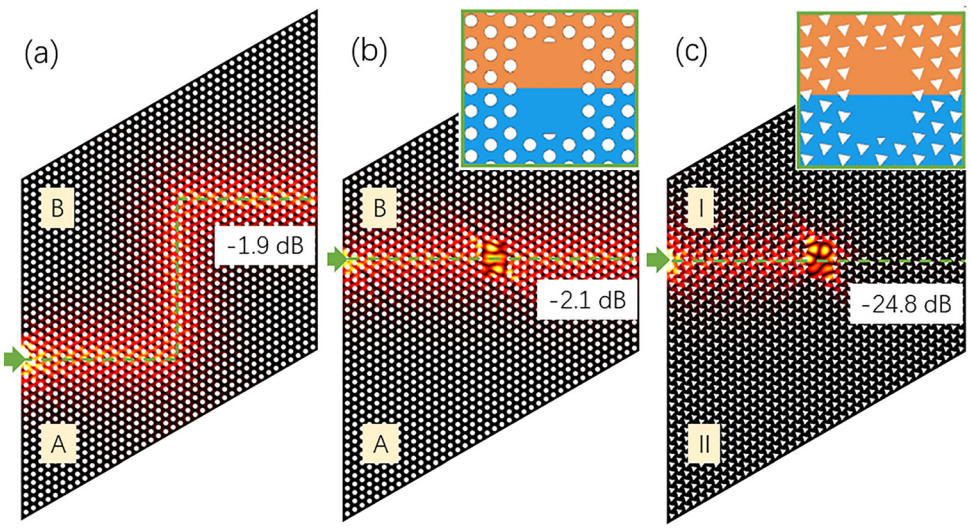

FIG. 4. Numerical simulation of interface mode transmission across finite samples. Pressure amplitude in the case of (a) 90° bending channel, (b) straight channel of the armchair type containing a defect, and (c) calculation of a classical VHE model for the same setup for comparison with (b). In (c), the triangular scatters rotates 10° (−10°) in domain I (II) and the excitation frequency is 3750 Hz. (Model parameters: lattice vector is 4.3 cm, the edge of triangular scatterer is 3 cm, and the bulk gap is 3600–4100 Hz). The insets zoom in on the SCs and defects.

for the B/A configuration at 4600 Hz (denoted by a circle on the band). Figure 3(d) shows the projected band structure of a strip supercell divided by an *armchair* domain wall along the *x*-direction; interface bands for A/B (upper A and lower B) and B/A configurations are similarly plotted. Again, an eigenstate at 4600 Hz for the B/A configuration is shown by the figure inset.

The interface band structure of the armchair domain wall here is remarkable. Usually, the interface modes on a zigzag domain wall are topologically well protected since the projections of inequivalent valleys are separated from each other. However, for VHE insulators with un-displaced valleys along the armchair domain wall, the projection of valley K and K′ coincides at $k_x = 0$ so that the opposite topological charges tend to annihilate. In this case, the two interface bands usually do not cross each other, essentially implying that they are not topologically protected.[14] In some designs of VHE insulator,[10,21] although a high transmission interface pathway can be achieved by including an armchair domain wall, it is more prone to backscattering when the wave encounters defects, as will be shown in Fig. 4. As a result, wave guides based on an ordinary VHE are more typically designed with bending angles that retain the zigzag domain wall.[16] In the present model, however, the magnitude and the direction of valley offset can be tuned at will to avoid overlap of valley projections and preserve a non-trivial topological charge, as indicated by the vertical dashed green lines in Fig. 3(d). In this case, the projected band diagram of the armchair wall possesses the same features as that of the zigzag. Therefore, robust interface transmission may be achieved equally for both the two types of domain wall owing to the suppression of inter-valley scattering. This will facilitate the design of more general topological channels.

To verify backscattering suppression and robust transmission of topological valley interface modes, we perform full-field frequency domain simulations on a finite lattice comprising 40×40 unit cells with the aid of a radiation boundary condition as shown in Fig. 4(a). A 90° bending channel composed of an armchair-zigzag-armchair domain wall is established using B/A phases. The left side input of the channel is excited by a Gaussian beam at a frequency of 4600 Hz located in the bulk gap. It is observed that the interface wave propagates with negligible backscattering and quite high transmission (−1.9 dB). Referring to Fig. 3, the propagating interface wave is unambiguously K′-valley projected for both types of wall; hence, it can smoothly traverse the channel corner. Furthermore, the transmission along the armchair channel can also be immune to defects for the present SC. As shown in Fig. 4(b), several scatterers are removed to create a rectangular defect in the middle of the armchair waveguide, and the numerical result reveals that the high transmission is almost unaffected (−2.1 dB). For comparison, Fig. 4(c) presents a simulation result of the same setup for a classical VHE model, composed of rotated triangular scatterers and a traditional acoustic fluid, for which the armchair interface mode is also supported, yet with weak topological protection. It is found that the wave is almost blocked by the defect (−24.8 dB transmission) due to backscattering.

In summary, we theoretically investigated an SC system exhibiting the VHE by using the acoustic media with Willis coupling. The vector nature of the Willis coupling parameter offers an alternative approach to lowering the SC symmetry and inducing a TP transition. It is revealed that the offset of Dirac cones and gapped valleys is intimately related to the direction of Willis coupling and can be utilized to achieve robust transmission along zigzag, armchair, and even more general types of domain walls. Although the realization of Willis acoustic media with strong coupling remains an ongoing topic of research, the unique features found in this study may stimulate further the exploration of both VHE and Willis metamaterials.

This work was supported by the National Natural Science Foundation of China (Grant Nos. 11972080, 11632003, and 11972083).

Published under an exclusive license by AIP Publishing

DATA AVAILABILITY

The data that support the findings of this study are available from the corresponding author upon reasonable request.

REFERENCES

[1]M. Z. Hasan and C. L. Kane, Rev. Mod. Phys. **82**, 3045 (2010).
[2]B. A. Bernevig, T. L. Hughes, and S. C. Zhang, Science **314**, 1757 (2006).
[3]F. D. Haldane, Phys. Rev. Lett. **61**, 2015 (1988).
[4]C. L. Kane and E. J. Mele, Phys. Rev. Lett. **95**, 226801 (2005).
[5]F. D. Haldane and S. Raghu, Phys. Rev. Lett. **100**, 013904 (2008).
[6]A. B. Khanikaev, S. H. Mousavi, W. K. Tse, M. Kargarian, A. H. MacDonald, and G. Shvets, Nat. Mater. **12**, 233 (2013).
[7]V. Peano, C. Brendel, M. Schmidt, and F. Marquardt, Phys. Rev. X **5**, 031011 (2015).
[8]Z. Wang, Y. Chong, J. D. Joannopoulos, and M. Soljačić, Phys. Rev. Lett. **100**, 013905 (2008).
[9]C. He, X. Ni, H. Ge, X. Sun, Y. B. Chen, M. Lu, X. Liu, and Y. Chen, Nat. Phys. **12**, 1124 (2016).
[10]J. Lu, C. Qiu, L. Ye, X. Fan, M. Ke, F. Zhang, and Z. Liu, Nat. Phys. **13**, 369 (2017).
[11]Z. Yang, F. Gao, X. Shi, X. Lin, Z. Gao, Y. Chong, and B. Zhang, Phys. Rev. Lett. **114**, 114301 (2015).
[12]S. Wang, G. Ma, and C. T. Chan, Sci. Adv. **4**, eaaq1475 (2018).
[13]M. Xiao, G. Ma, Z. Yang, P. Sheng, Z. Q. Zhang, and C. T. Chan, Nat. Phys. **11**, 240 (2015).
[14]Y. Yang, Z. Yang, and B. Zhang, J. Appl. Phys. **123**, 091713 (2018).
[15]Z. Zhang, Y. Tian, Y. Wang, S. Gao, Y. Cheng, X. Liu, and J. Christensen, Adv. Mater. **30**, 1803229 (2018).
[16]M. P. Makwana and R. V. Craster, Phys. Rev. B **98**, 235125 (2018).
[17]S. H. Mousavi, A. B. Khanikaev, and Z. Wang, Nat. Commun. **6**, 8682 (2015).
[18]L. M. Nash, D. Kleckner, A. Read, V. Vitelli, A. M. Turner, and W. T. Irvine, Proc. Natl. Acad. Sci. **112**, 14495 (2015).
[19]J. Vila, R. K. Pal, and M. Ruzzene, Phys. Rev. B **96**, 134307 (2017).
[20]Y. Chen, X. Liu, and G. Hu, J. Mech. Phys. Solids **122**, 54 (2019).
[21]M. Yan, J. Lu, F. Li, W. Deng, X. Huang, J. Ma, and Z. Liu, Nat. Mater. **17**, 993 (2018).
[22]Q. Zhang, Y. Chen, K. Zhang, and G. Hu, Phys. Rev. B **101**, 014101 (2020).
[23]D. Xiao, W. Yao, and Q. Niu, Phys. Rev. Lett. **99**, 236809 (2007).
[24]J. Lu, C. Qiu, M. Ke, and Z. Liu, Phys. Rev. Lett. **116**, 093901 (2016).
[25]S. Li, I. Kim, S. Iwamoto, J. Zang, and J. Yang, Phys. Rev. B **100**, 195102 (2019).
[26]B. Xia, S. Zheng, T. Liu, J. Jiao, N. Chen, H. Dai, D. Yu, and J. Liu, Phys. Rev. B **97**, 155124 (2018).
[27]X. Han, L. Li, Y. Hu, L. Ling, Z. Geng, Y. Peng, D. Zhao, X. Zhu, and X. Wang, Phys. Rev. Appl. **14**, 024091 (2020).
[28]G. W. Milton, M. Briane, and J. R. Willis, New J. Phys. **8**, 248 (2006).
[29]J. R. Willis, Wave Motion **3**, 1 (1981).
[30]J. R. Willis, *Continuum Micromechanics* (Springer, 1997), pp. 265–290.
[31]C. F. Sieck, A. Alù, and M. R. Haberman, Phys. Rev. B **96**, 104303 (2017).
[32]M. B. Muhlestein, C. F. Sieck, A. Alu, and M. R. Haberman, Proc. R. Soc. A **472**, 20160604 (2016).
[33]M. B. Muhlestein, C. F. Sieck, P. S. Wilson, and M. R. Haberman, Nat. Commun. **8**, 15625 (2017).
[34]J. Li, C. Shen, A. Diaz-Rubio, S. A. Tretyakov, and S. A. Cummer, Nat. Commun. **9**, 1342 (2018).
[35]A. Merkel, V. Romero-García, J. Groby, J. Li, and J. Christensen, Phys. Rev. B **98**, 201102 (2018).
[36]Y. Chen, X. Li, G. Hu, M. R. Haberman, and G. Huang, Nat. Commun. **11**, 3681 (2020).
[37]S. Koo, C. Cho, J. Jeong, and N. Park, Nat. Commun. **7**, 13012 (2016).
[38]L. Quan, Y. Ra'di, D. L. Sounas, and A. Alù, Phys. Rev. Lett. **120**, 254301 (2018).
[39]A. Melnikov, Y. K. Chiang, L. Quan, S. Oberst, A. Alù, S. Marburg, and D. Powell, Nat. Commun. **10**, 3148 (2019).
[40]All simulations in the paper were carried out by the pressure acoustic module of the commercial finite-element software package COMSOL Multiphysics. To simulate the wave behavior of a Willis acoustic fluid, the original weak form of the Helmholtz equation should be modified for the wave equation of a Willis material; see M. B. Muhlestein, B. M. Goldsberry, A. N. Norris, and M. R. Haberman, Proc. R. Soc. A **474**, 20180571 (2018).
[41]J. Lu, C. Qiu, S. Xu, Y. Ye, M. Ke, and Z. Liu, Phys. Rev. B **89**, 134302 (2014).
[42]Symmetry operations with an invariant SC form a point group G, e.g., $C_{n(v)}$ means $2\pi/n$ rotations (plus a reflection). However, the property of Bloch states is related to the point group of the wave vector, G_k (subgroup of G), containing operations that take k into itself or its equivalent one. The dimension of the irreducible matrix representation of Gk implies degeneracies or cones in the band structure; see, e.g., M. S. Dresselhaus, D. Dresselhaus, and A. Jorio, *Group Theory: Application to the Physics of Condensed Matter* (Springer-Verlag, Berlin/Heidelberg, 2008).

Published under an exclusive license by AIP Publishing